ELSEVIER

Journal of Electroanalytical Chemistry 383 (1995) 67–74

JOURNAL OF ELECTROANALYTICAL CHEMISTRY

Interface condition of n-Si(111) during photocurrent oscillations in NH_4F solutions

M. Aggour, M. Giersig, H.J. Lewerenz

Hahn-Meitner-Institut, Bereich Photochemische Energieumwandlung, Glienicker Strasse 100, D-14109 Berlin, Germany

Received 22 July 1994

Abstract

Photocurrent oscillations at n-type Si(111) were investigated in ammonium fluoride solutions by in situ ellipsometry and ex situ transmission electron microscopy (TEM) experiments. In situ ellipsometric data show that the current oscillations are concomitant with fluctuation of the optical parameters Δ and Ψ. TEM analysis revealed the presence of pores in the silicon oxides during the oscillations. Effective medium theory following Bruggemann's formalism was used to evaluate the change in refractive index and thickness of the anodic oxide film. The observed fluctuation in Δ and Ψ can be explained by changes in refractive index of the oxide due to the opening and closing of pores.

Keywords: Photocurrent oscillations; n-Si(111); NH_4F

1. Introduction

Spontaneous oscillations have been observed in electrochemical as well as chemical systems [1–3], but their origins remain largely conjectural. The appearance of current oscillations of silicon in fluoride-containing solution at high potentials was mentioned early by Turner [4] and was addressed recently by several authors [5–15]. Few studies have been directed towards investigation of the phenomenon itself.

Gerischer and Lubke [5] suggested that the appearance of oscillations can be caused by a non-linear correlation between formation and dissolution of the oxide. Zhang et al. [8] have proposed a competition between surface islands of oxide dissolution and free silicon dissolution. Ozanam and coworkers [9, 10] have attributed the oscillations to local fluctuations in the thickness of the surface oxide. They argue that the surface consists of a juxtaposition of small self-oscillating areas synchronized by a potential perturbation giving rise to macroscopic oscillations. They have found that these oscillations can be damped or sustained by adding an external resistor in series with the sample [11]. The microscopic or chemical nature of the oscillations, however, was not detailed. Föll [12] suggested that the presence of a dielectric layer could be responsible for the oscillations. Recently a connection to chaos theory was established [13]. Lehmann and Gösele [14] reported the existence of stable and predictable current (potential) oscillations for the silicon|HF system at positive potentials far into the electropolishing regime. Lewerenz and Schlichtörl [15] observed stationary oscillations in the photocurrent and excess microwave reflectivity complementary to each other and they proposed the possibility of a spatially anisotropic thickness during the oscillations.

In spite of extensive study of the oscillation phenomenon, a detailed description of the interrelation between the photocurrent oscillation and physicochemical events at the silicon|electrolyte phase boundary has not yet been attempted. In earlier work we suggested a model based on the fluctuation of pores within the oxide in order to explain qualitatively the pronounced photocurrent modulation [16] despite a relatively small variation in oxide thickness [17]. The model proposed is inspired by the charge-collection principle in point contact silicon solar cells which is based on the spatial distribution of charge-collecting centers.

In order to attain more specific information on the interfacial processes to develop the above model, we applied a combination of electrochemical in situ ellipsometry and transmission electron microscopy (TEM) to investigate the oscillatory behaviour of the anodic

SSDI 0022-0728(94)03723-X

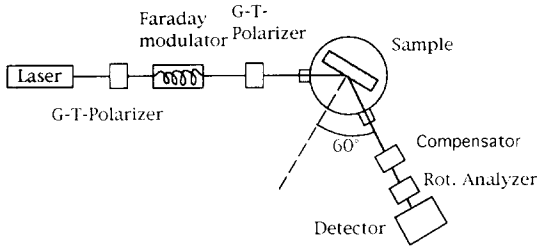

Fig. 1. Schematic representation of the rotating analyser ellipsometer.

dissolution of silicon in ammonium fluoride media. The photocurrent oscillations were followed by monitoring simultaneously the ellipsometric parameters Δ and Ψ, which allow evaluation of the thickness and refractive index of optically transparent films. The oxide layer on Si(111) during photocurrent oscillation was investigated by TEM experiments. In the present work, we provide morphological information necessary to investigate the validity of this model [16].

2. Experimental section

2.1. Ellipsometry

Fig. 1 shows a block diagram of the ellipsometer used. The instrument works in the rotating analyser mode [18]. The incoming linear polarized light of an He–Ne laser (λ = 6328 Å, P = 4.1 mW) was modulated with a Faraday modulator positioned between two crossed polarizers (Glan-Thompson prisms). The reflected light, with its polarization altered by the optical properties of the sample, passes through the compensator, the rotating analyser and then strikes the Si detector (EG&G SGD-444). The polarizers and analyser were driven by step motors. The analyser was rotated in discrete steps, changing the orientation by 4.5° per step. By applying an alternating current to the Faraday modulator, the probe light intensity could be reduced down to the nanowatt range. Owing to the intensity modulation of the probe light (2422 Hz) and phase sensitive detection, reliable readings even at low light intensities were obtained. This enables us to take ellipsometric measurements at probe light intensities at which photoinduced interface alterations are negligible [18]. Measurement control and computations were performed using an IEC-bus system with a HP 300 computer allowing the simultaneous recording of the current, the ellipsometric parameters Δ and Ψ and the reflected absolute light intensity. An additional roughness parameter can be derived from the higher coefficients of Fourier analysis of ellipsometric intensity data [19].

The photoelectrochemical treatment was carried out in a specially designed polypropylene vessel (Fig. 1). The cell windows were made of quartz. Since the time resolution between successive ellipsometric measurements is 64 s at our low probe light levels, the period of sustained current oscillation had to be increased. Therefore we performed the experiments with 0.1 M NH_4F, pH 4.6 at a positive potential of 6 V (SCE) resulting in a period of 350 s.

2.2. Sample and electrolyte preparation

The n-Si(111) samples used in the experiments were phosphorus doped with resistivities in the range 4 to 12 Ω cm range. Ohmic back contacts were made by rubbing Ga/In alloy on to the back side of the crystal.

For in situ ellipsometric investigations the samples were sandwiched between two polypropylene blocks using Teflon o-rings as seals. The electrochemical measurements were taken using a platinum counter electrode and saturated calomel electrode (SCE) as reference electrode. Electrical control was provided by a potentiostat-galvanostat (Heka model 128). Electrolytes were prepared from ammonium fluoride and purified water (milli UF, Millipore). The pH was adjusted by the addition of concentrated H_2SO_4. For sample illumination a tungsten-halogen lamp was used. Prior to the experiments the cell was cleaned intensively in $HNO_3 + H_2O_2 + H_2O$ (1:1:1).

To achieve defined surface conditions, the primary treatment consisted of a photoelectrochemical oxidation in 0.1 M NH_4F at pH 4.0 (U = 6 V) and illumination with white light (50 mW cm^{-2}) under the conditions of photocurrent oscillation for 15 min. Then the oxide layer was removed in the absence of light without a change in the applied potential.

2.3. Transmission electron microscopy

To interrup the electrochemical conditioning of the silicon crystal for TEM investigation, the sample was removed under potential from the electrolyte and rinsed intensively with triple distilled water for 10 s. The surface region was removed mechanically by slicing with a razor blade. A 50 Å thick amorphous carbon film was used as support, and the system was examined in a Philips CM 12 transmission electron microscope, which was equipped with a 9800 EDAX analyser. The acceleration voltage was 120 kV. The lateral resolution was 1.8 Å.

3. Combined ellipsometric–electrochemical investigation

The SiO_2 etching rate in fluoridic solutions depends on the concentration of HF_2^- and undissociated HF

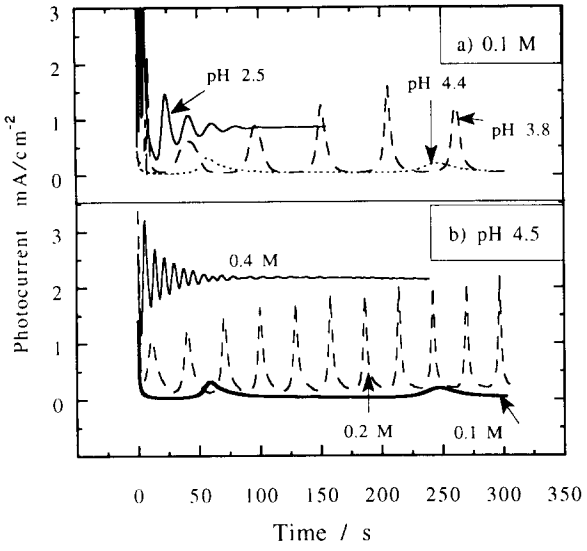

Fig. 2. Photocurrent oscillations on illuminated n-Si: (a) in 0.1 M NH_4F for different pH; (b) in 0.1 M, 0.2 M and 0.4 M NH_4F at pH 4.5; light intensity 70 mW cm^{-2}, electrode potential +6 V (SCE).

species [20]. The concentration of F^-, HF_2^- and HF can be evaluated according to,

$$K_1[HF] = [H^+][F^-] \quad (1)$$

$$K_2[HF_2^-] = [HF][F^-] \quad (2)$$

In Eqs. (1) and (2), $[HF_2^-]$, [HF], $[F^-]$ and $[H^+]$ denote the concentrations of the fluoridic species and the proton concentration respectively. A summary of experimentally obtained equilibrium constants K_1, K_2 is given in Ref. [21]. Since the oxide etching rate depends on the molarity and acidity of the electrolyte, we varied the pH and the concentration of the aqueous NH_4F solution to study the influence of the SiO_2 etching rate on the oscillatory behaviour of the photocurrent.

Fig. 2 shows the temporal variation of the photocurrent of n-Si in ammonium fluoride solution for a variety of electrolyte compositions and pH under potentiostatic control (6 V). In Fig. 2(a) the photocurrent density in 0.1 M NH_4F at different pH is presented. It can be seen that the frequency of the oscillations becomes larger in more acidic solutions. The frequency also varied with the fluoride concentration (Fig. 2(b)). Here the pH was kept constant at 4.5. With an increase in the concentration (which results in a higher oxide etching rate) the frequency of the sustained oscillations rises. In more concentrated ammonium fluoride solutions (above 0.4 M) the oscillations disappear and we observe evolution of gas at the counter electrode. It can be seen from Figs. 2 and 3 that the amplitude of the oscillations varied with time, and for strongly damped oscillations ($T < 50$ s) (Fig. 2) a gradual decay to a stationary current is observed. However, for sustained oscillations ($T > 50$ s) (Fig. 3(b)), the amplitude increases, reaches a maximum and decays with a somewhat smaller absolute slope compared with the increase in amplitude.

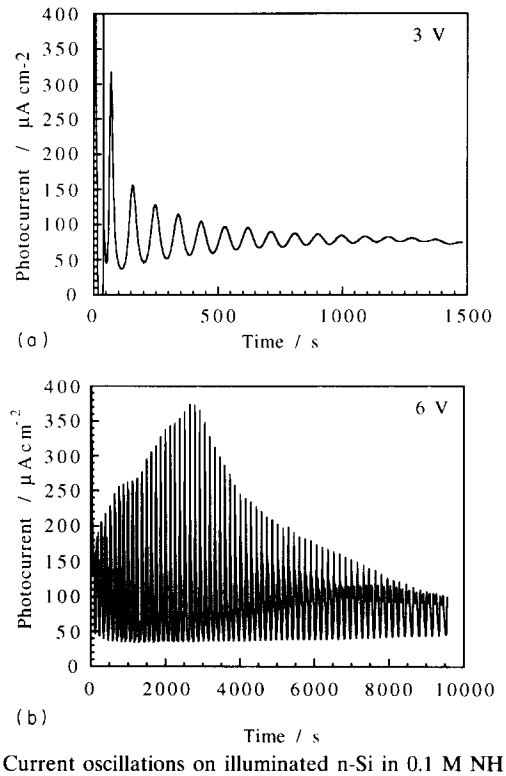

Fig. 3. Current oscillations on illuminated n-Si in 0.1 M NH_4F, pH 4.0, light intensity 70 mW cm^{-2}, electrode potentials (a) +3 V and (b) +6 V (SCE).

Note that the frequency of the oscillations is almost unaffected by the applied bias [5] which is not the case for the amplitude. The results of potentiostatic experiments at 0.1 M NH_4F and pH 4.0 are summarized in Fig. 4. The data show the depth of modulation of the photocurrent oscillations by plotting the difference between the maxima and minima of the photocurrent as a

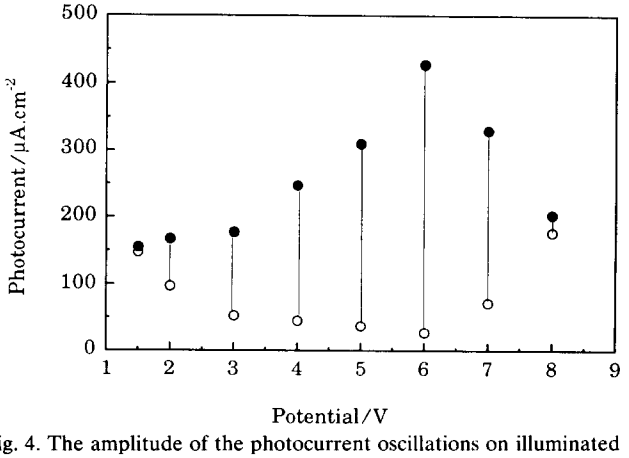

Fig. 4. The amplitude of the photocurrent oscillations on illuminated n-Si as a function of the applied potential in 0.1 M NH_4F at pH 4.0, light intensity 70 mW cm^{-2}.

function of electrode potential, as indicated by the ends of vertical bars. Below 1.5 V and above 8 V (SCE), oscillations were not observed. In these non-oscillatory regions an initial transient was observed followed by a steady-state current value. In the range $1.5\ V \leq V < 8\ V$, oscillatory current behaviour is always observed; the amplitude of the oscillations increases with applied anodic potential, reaches a maximum around 6 V and then diminishes as shown in Fig. 4.

The duration of the oscillations in 0.1 M NH_4F at pH 4.4, for instance, is larger by a factor of 60 compared with a solution of pH 2.5 (Fig. 2(a)). The same factor is observed for 0.4 M NH_4F and 0.1 M NH_4F, both at the same pH 4.5 (Fig. 2(b)). Therefore, the stationary limit is only shown for the more strongly damped oscillations. The applied potential also influences the time at which the oscillations start and stop (Figs. 3, 4).

The above results demonstrate that the observed oscillatory photocurrent must be due to electronic and/or morphological structural changes at the electrode surface (i.e. surface morphology, film thickness, or film structure). As described previously [16], the etch rate for anodic oxides is directly proportional to the oscillation frequency for a large variety of concentrations and pH. This connects the oscillation frequency to oxide removal processes.

Under the condition of sustained oscillations, the amplitude as well as the frequency remain unchanged for several tens of minutes. This enabled us to perform an in situ ellipsometric investigation of the silicon | electrolyte interface.

The experimental Δ and Ψ values from in situ ellipsometry of oxidation on an illuminated n-Si sample in 0.1 M NH_4F, pH 4.6 at the potential of 6 V (SCE) are shown in Fig. 5.

It is evident from Fig. 5 that Δ and Ψ oscillate with the photocurrent. The ellipsometric parameter Δ is in opposite phase with Ψ, and the photocurrent is almost in phase with Ψ but exhibits a phase shift of some degrees. The variation of Δ shows distinct differences in comparison with the lineshape of the current density around the minima. For instance, the amplitude of Δ displays a somewhat asymmetric behaviour which is not seen in the current oscillations. In contrast to the photocurrent we can observe that the minimum and maximal value of Δ increase with time. However within one period the drop in Δ is much more pronounced. The changes in Δ (unlike those obtained for p-Si [17]) are remarkably high, indicating that the photocurrent oscillations could be the consequence of build-up and removal of the anodic oxide.

First we tried to model the changes in Δ and Ψ via changes in oxide thickness in a three-layer system consisting of a semi-infinite crystalline Si substrate, an amorphous SiO_2 film and an aqueous NH_4F ambient.

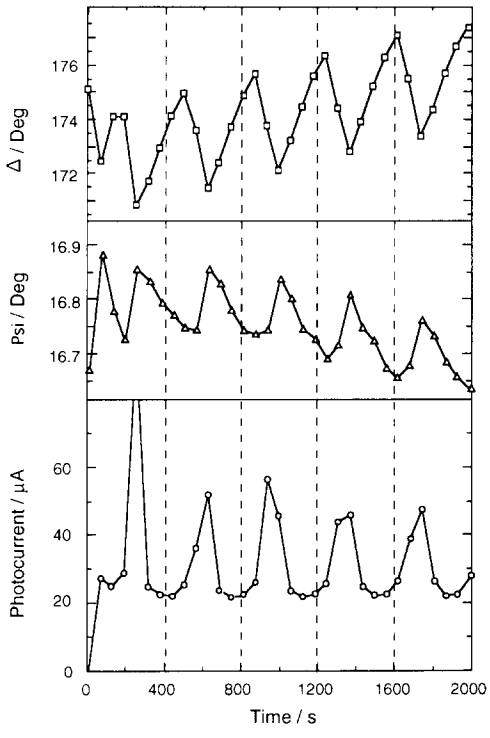

Fig. 5. Changes in photocurrent I_{ph} and ellipsometric parameters Δ and Ψ measured during current oscillations on illuminated n-Si in 0.1 M NH_4F, pH 4.6, light intensity 80 mW cm^{-2}, electrode potential +6 V (SCE).

The functional dependence of Δ and Ψ on the system parameters can be written as [22]

$$\tan(\Psi)\exp(i\Delta) = r(n_0, n_1, n_s, d, \Phi, \lambda) \tag{3a}$$

$$= \frac{r_{1p} + r_{2p}\,e^{-2i\delta}}{1 + r_{1p}r_{2p}\,e^{-2i\delta}} \frac{r_{1s} + r_{2s}\,e^{-2i\delta}}{1 + r_{1s}r_{2s}\,e^{-2i\delta}} \tag{3b}$$

where n_0, n_1 and n_s are the complex refractory indices of the ambient, film and the substrate respectively, and d denotes the thickness of the film. Φ is the angle between the incident beam and the surface normal to the sample, r_{1p}, r_{1s}, r_{2p} and r_{2s} are the Fresnel coefficients for reflection at the ambient | film interface and at the film | substrate interface respectively. The film thickness appears in the quantity δ which is the change in phase of the beam caused by traversing the film of thickness d and index of refraction n_1:

$$\delta = \frac{4\pi}{\lambda} d\left(n_1^2 - \sin^2\Phi\right)^{1/2} \tag{4}$$

With n_0, Φ and λ as experimentally controlled variables and with n_s fixed with either n_1 or d, the other parameter can be determined from the measured values of Δ and Ψ. Optical constants for Si [23] and SiO_2 [24,25] were taken from the literature. The refrac-

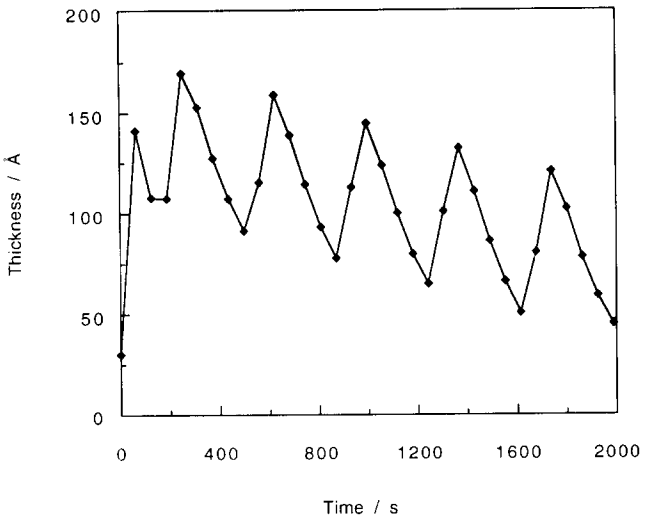

Fig. 6. Calculated thickness of the film from the measured parameters Δ and Ψ using the ideal ambient–film–substrate model with a constant refractive index for the oxide ($n = 1.45$).

tive index of the electrolyte was obtained from the data for pure H_2O ($n_0 = 1.333$) [26].

The ellipsometric data Δ and Ψ allow calculation of the temporal behaviour of the film thickness [27]. In Fig. 6 the evaluated film thickness is shown as a function of time (the refractive index of the oxide is assumed constant $n_{ox} = 1.457$). The fluctuations in d are almost 70 Å, and they are similar to that observed in Δ (Fig. 5) but in the opposite phase. Whenever d is minimized, Δ is high, Ψ is small and the photocurrent is in the increasing mode. Similar results were obtained for photocurrent oscillations in 0.1 M NH_4F, pH 4.0 at +6 V.

The above model results in pronounced changes in thickness of the oxide. Such changes should be easily detectable by coverage analysis X-ray photoelectron spectroscopy (XPS) [28] performed in the combined electrochemistry–ultrahigh vacuum analysis system described earlier [29,30]. For better interruption of the oscillation, the period of the photocurrent oscillations was reduced to a value of about 50 s using 0.1 M NH_4F at pH 4.0 at positive potentials of 5 V vs. SCE and a light intensity of 100 mW cm^{-2}. The anodization was interrupted at the photocurrent maximum (a) and minimum (b) (see Fig. 7).

Fig. 8 shows XP spectra of the O 1s line for surface situation (a) (spectrum (a)) and (b) (spectrum (b)). The symmetric peak at −534.45 eV in spectrum (a) can be assigned to oxygen in SiO_2 structures [31]. Emissions from silicon hydroxides which are expected at a binding energy of −532.6 eV [32] cannot be resolved owing to the broad SiO_2-related intensity. In spectrum (b) the O 1s peak is present at −534.35 eV which is about 100 meV smaller than the value for spectrum was (a). Some emission from the F 1s level is found which is not shown here but was taken into account in the coverage

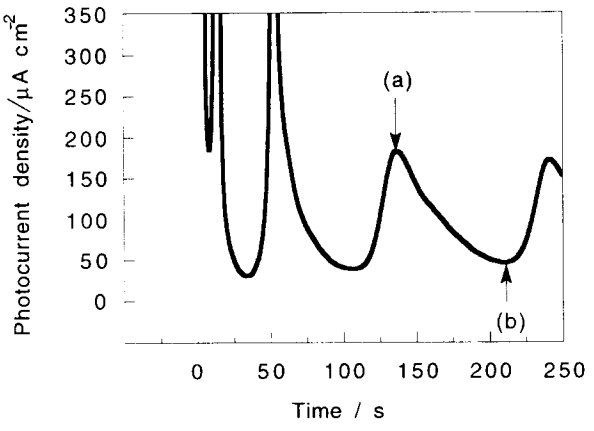

Fig. 7. Temporal behaviour of the photocurrent. Labels (a) and (b) denote emersion times.

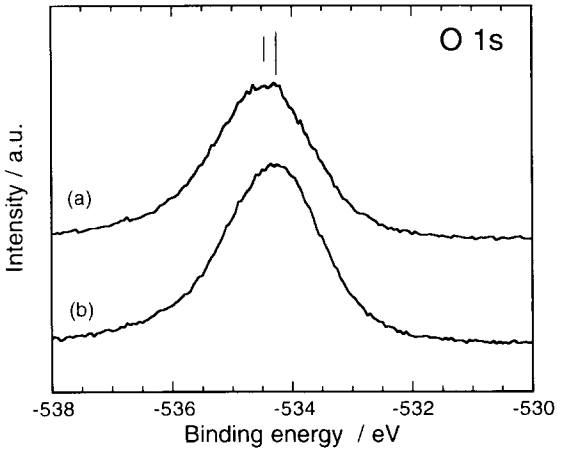

Fig. 8. Photoelectron yields in the O 1s core-level region; spectrum (a) was recorded for the surface at photocurrent maximum and spectrum (b) for the current minimum. The solution was 0.1 M NH_4F, pH 4.0, light intensity 70 mW cm^{-2}, electrode potential +5 V (SCE).

calculation; for determination of the chemical composition and thickness of the oxidic film a coverage analysis was carried out assuming a closed overlayer with homogenous morphological structure and chemical composition [33–36]. The results are summarized in Table 1 [28].

Data analysis using the well known fractional and closed overlayer models [33] shows that the film thick-

Table 1
Evaluated thickness and composition of the oxidic overlayer growth in Si(111) in 0.1 M NH_4F, pH 4.0, light intensity 70 mW cm^{-2}, electrode potential +5 V (SCE) at maximum (a) and minimum (b) of photocurrent oscillations

Condition	Thickness d/Å	$SiO_{2-x}F_y$	
		x	y
a	41	0.45±0.1	0.2
b	39	0.45±0.1	0.2

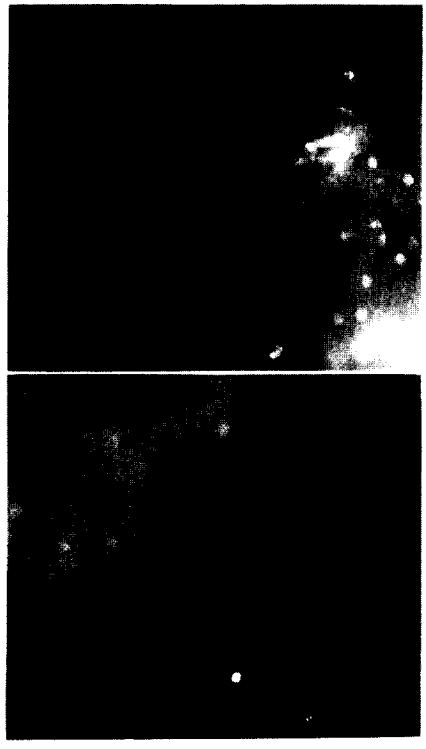

Fig. 9. Typical TEM images of the silicon oxide layers recorded on illuminated n-Si at photocurrent maximum (a) and minimum (b). The solution was 0.1 M NH_4F at pH 4.0. The pores can clearly be recognized.

ness and the chemical composition of the film remain almost constant. Hence the assumptions used above which were based on growth and removal of oxide layers cannot easily be maintained even if one assumes that a substantial part of the oxide consists of hydroxide groups and water. In our earlier publication [16] we postulated that the photocurrent modulation could originate from the opening and closing of quite small surface regions (pores in the oxide) since the collection efficiency through such contacts is high owing to the large diffusion length of carriers in Si. In order to gain additional morphological information, we performed TEM measurements at the photocurrent minima and maxima.

4. Transmission electron microscopy

For TEM analysis, the anodization was interrupted at the photocurrent maximum (a) and minimum (b) (Fig. 7). Fig. 9 shows the typical morphology of the silicon oxide layers formed during anodic polarization (6 V) in 0.1 M NH_4F, pH 4.0. A porous oxide layer is formed. The pores are distributed across the whole layer, and their sizes are almost identical for a given condition. From these micrographs the pore diameter were measured and the average values were obtained

Table 2
Measured pore diameter and density from TEM during current oscillations on illuminated n-Si in 0.1 M NH_4F, pH 4.0, electrode potential +6 V (SCE), at maximum (a) and minimum (b) of photocurrent oscillations

Condition	Diameter/Å	Density/cm^{-2}	Volume/%
a	90–130	$1.8\ 10^{11}$	0.102
b	60–80	$9\ 10^{10}$	0.018

from about 50 measurements (Table 2). As seen in Fig. 9, the porosity increases with current. The average pore diameters at position (a) amount to 120 Å and the pore density to 1.8×10^{11} pores cm^{-2}. By position (b) the diameter and the density have decreased to 70 Å and 9×10^{10} pores cm^{-2} respectively. The ultra structures of the formed pores and their properties will be reported in a subsequent publication [37].

5. Micromorphology and photocurrent oscillations

The XPS and TEM data (Figs. 8,9) indicate serious problems with the assumption of a periodic variation in thickness of an oxidic layer as evaluated in Fig. 6 to account for the periodic changes in Δ and Ψ. We therefore attempted to evaluate the in situ ellipsometry data on the basis of the morphological information provided by the TEM results shown in Fig. 9. In addition, the existence of a transition region [38] of suboxides SiO_x ($x < 2$) has to be considered as shown schematically in Fig. 10. The characteristic range for this region is about 0.2–2 nm in thickness [39], and the optical properties depend on x [40]. The ellipsometric data are analysed assuming the oxide layer to be a composite mixture of silicon (Si roughness), silicon oxide and electrolyte (water, hydroxide) (see Fig. 10). We used the effective medium approximation (EMA) of Bruggeman [41] (random mixture). In this approxi-

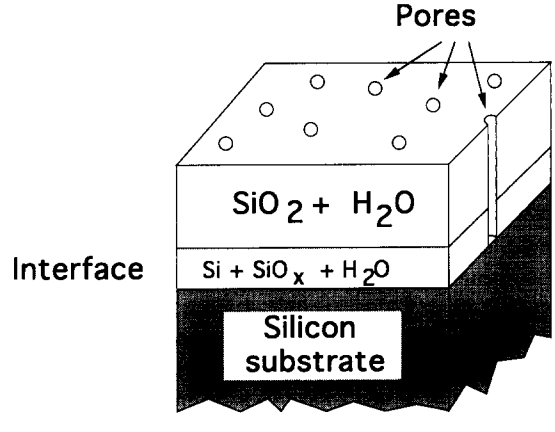

Fig. 10. Model for the substrate–interface–overlayer and electrolyte system.

mation the effective medium dielectric function ϵ_e is given by

$$0 = \sum_{i=1}^{N} f_i \frac{\epsilon_i - \epsilon_e}{\epsilon_i + 2\epsilon_e} \quad (5)$$

where N is the number of distinct media in the mixture; f_i and ϵ_i are the volume fraction and dielectric function of the ith component respectively. Silicon, the oxide and the electrolyte have volume fractions f_1, f_2 and $(1-f_1-f_2)$ respectively. The classical Bruggeman formulation, for spherical inclusions, is deduced using Eq. (5)

$$0 = f_1(\epsilon_1 - \epsilon_e)(\epsilon_2 + 2\epsilon_e)(\epsilon_3 + 2\epsilon_e) + f_2(\epsilon_2 - \epsilon_e)(\epsilon_1 + 2\epsilon_e)(\epsilon_3 + 2\epsilon_e) + (1 - f_1 - f_2) \times (\epsilon_3 - \epsilon_e)(\epsilon_1 + 2\epsilon_e)(\epsilon_2 + 2\epsilon_e) \quad (6)$$

After rearrangement this can be written

$$A\epsilon_e^3 + B\epsilon_e^2 + C\epsilon_e + D = 0 \quad (7)$$

where

$$A = -4$$

$$B = 2(-3f_2 - 3f_1 + 2)\epsilon_3 + (3f_2 - 1)\epsilon_2 + (3f_1 - 1)(3f_2 - 1)\epsilon_2\epsilon_1$$

$$C = (3f_1 + 3f_2 + 2)\epsilon_1\epsilon_2 + (2 - 3f_2)\epsilon_1\epsilon_3 + (2 - 3f_1)\epsilon_2\epsilon_3$$

$$D = \epsilon_1\epsilon_2\epsilon_3$$

The influence of the volume fraction of the electrolyte in the film on the effective dielectric constant ϵ_e is shown in Fig. 11. The refractive index ($n^2 = \epsilon_e$) decreases with increasing volume fraction of the dielectric in the film and increases with increasing volume fraction of silicon. The effective dielectric constant ϵ_e is then dependent on the number of pores, their radii and depth and on the Si surface protrusions (Si roughness). For example, a change in the volume of H_2O of 20% in the oxide causes a change in the effective refractive index of 0.025, and the incorporation of 10% Si as roughness in the oxide increase the effective refractive index 0.16 (Fig. 11). Therefore there is a high sensitivity in n, i.e. in both Δ and Ψ, to the presence of an interface layer.

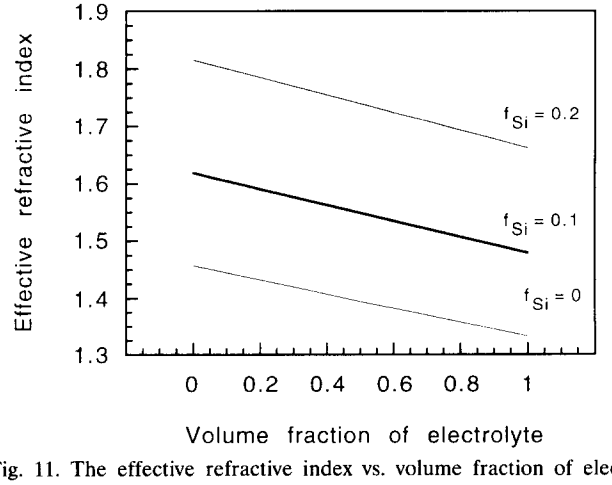

Fig. 11. The effective refractive index vs. volume fraction of electrolyte at different volume fraction of silicon f_{Si}.

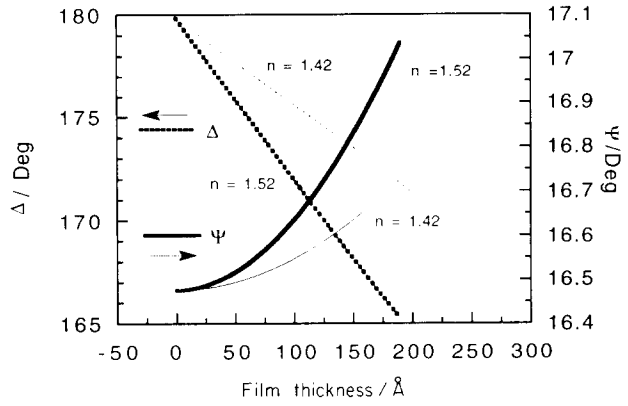

Fig. 12. Values of the ellipsometric parameters Δ and Ψ as a function of the oxide thickness for transparent films on Si with effective refractive indices $n = 1.52$ and $n = 1.42$.

Fig. 12 shows the calculated Δ (dotted lines) and Ψ (solid lines) of the oxides as a function of film thickness for two different refractive indices which were obtained assuming a porous oxide including SiO_2, H_2O and Si. The value $n = 1.42$ corresponds to an oxide with 80% SiO_2 and 20% H_2O. The refractive index $n = 1.52 - 0.0006i$ was calculated assuming a film configuration of 5% Si, 85% SiO_2 and 10% H_2O. As shown in Fig. 12, the difference $\Delta(n = 1.42) - \Delta(n = 1.52)$ and $\Psi(n = 1.42) - \Psi(n = 1.42)$ increases with the film thickness, i.e. with the applied potential. Taking into consideration the experimental results in the two oscillation positions (a) at maximum and (b) at minimum) (see Fig. 7, Tables 1 and 2), we come to the conclusion that only the change in refractive index can result in an oscillation of Δ and Ψ between the two corresponding curves where the morphology of the oxide passes periodically from one situation to the other. The model proposed explains the increase in amplitude of the photocurrent oscillation with the potential (Fig. 4) but cannot justify the decreases observed above 6 V. There is no doubt that the optical properties of the growth film are different in this region. This work continues in our laboratory with the objective of refining the model.

6. Conclusions

In situ ellipsometry, XPS and TEM measurements have been performed to elucidate the physicochemical origin of photocurrent oscillations on n-Si(111). TEM

data show pores in the oxide which vary in size and number in relation to the current minima and maxima. The ellipsometric data can be modelled using EMA assuming pores of varying volume within the oxide. The overall oxide thickness remains almost unaffected as shown by XPS. The findings support the so-called fluctuating pore model [16]

Acknowledgement

The authors are grateful to Dr. T. Bitzer for his contributions and Dr. A. Ennaoui for helpful discussion. This work was supported by the BMFT (grant No. 0328926A) and by the DAAD (M. Aggour).

References

[1] M. Thalinger and M. Volmer, Z. Phys. Chem., 150 (1930) 401.
[2] U.F. Frank and R. FitzHugh, Z. Elektrochem., 65 (1961) 156.
[3] R.J. Field and M. Burger, Oscillations and Traveling Waves in Chemical Systems Wiley, New York, 1985.
[4] D.R. Turner, J. Electrochem. Soc., 105 (1958) 402.
[5] H. Gerischer and M. Lübke, Ber. Bunsenges. Phys. Chem., 92 (1988) 573.
[6] V. Lehmann and H. Föll, J. Electrochem. Soc., 137 (1990) 653.
[7] D.J. Blackwood, A. Borazio, R. Greef, L.M. Peter and J. Stumper, Electrochim. Acta, 37 (1992) 889.
[8] X.G. Zhang, S.D. Collins and R.L. Smith, J. Electrochem. Soc., 136 (1989) 1561.
[9] J.-N. Chazalviel and F. Ozanam, J. Electrochem. Soc., 139 (1992) 2501.
[10] F. Ozanam, J.-N. Chazaviel, A. Radi and M. Etman, Ber. Bunsenges. Phys. Chem., 95 (1991) 98.
[11] J.-N. Chazalviel, F. Ozanam, M. Etman, F. Paolucci, L.M. Peter and J. Stumper, J. Electroanal. Chem., 327 (1992) 343.
[12] H. Föll, Appl. Phys. A, 53 (1991) 8.
[13] M.R. Bassett and J.L. Hudson, J. Electrochem. Soc., 137 (1990) 922.
[14] V. Lehmann and U. Gösele, Appl. Phys. Lett., 58 (1991) 856.
[15] H.J. Lewerenz and G. Schlichthörl, J. Electroanal. Chem., 327 (1992) 85.
[16] H.J. Lewerenz and M. Aggour, J. Electroanal. Chem., 8 (1993) 2548.
[17] J. Stumper, R. Greef and L.M. Peter, J. Electroanal. Chem., 310 (1991) 445.
[18] L. Cramer, H. Duwe, H. Jungblut, P. Lange and H.J. Lewerenz, J. Phys. Condens. Matter, 3 (1991) S77.
[19] H. Duwe, Dissertation, TU Berlin, 1992.
[20] J.S. Judge, J. Electrochem. Soc., 118 (1971) 1772.
[21] D. Koschel (Ed.), Fluor. In Gmelin Handbook of Inorganic Chemistry, Suppl. Vol. 3, Springer, Berlin, 1982.
[22] R.M.A. Azzam and N.M. Bashara, Ellipsometry and Polarized Light, North-Holland, Amsterdam, 1988.
[23] D.E. Aspnes and A.A. Studna, Phys. Rev. B, 27 (1983) 985.
[24] W.-K. Paik and J.O. Bockris, Surf. Sci. 28 (1971) 61.
[25] E.D. Palik, (ed.) Handbook of Optical Constants of Solids, Academic Press, Orlando, FL, 1985.
[26] R.C. Weast and M. J. Astle (eds.), Handbook of Physics and Chemistry, CRC Press, Boca Raton, FL, 1980–1981.
[27] S.S. So and K. Vedam, J. Opt. Soc. Am., 62 (1972) 16.
[28] T. Bitzer and H.J. Lewerenz, to be published.
[29] T. Bitzer and H.J. Lewerenz, Surf. Sci., 269–270 (1992) 886.
[30] H.J. Lewerenz and T. Bitzer, J. Electrochem. Soc., 139 (1992) L21.
[31] C.D. Wagner, W.M. Riggs, L.E. Davis and J.F. Moulder, Handbook of X-Ray Photoelectron Spectroscopy, Perkin-Elmer, Eden Prairie, MN, 1978.
[32] J.A. Schaefer, J. Anderson and G.J. Lapeyre, J. Vac. Sci. Technol. A, 3 (1985) 1443.
[33] D. Briggs and M.P. Seah, Practical Surface Analysis, Wiley, New York, 1983.
[34] F.J. Himpsel, P. Heimann and D.E. Eastman, Phys. Rev. B, 24 (1981) 2003.
[35] S. Ciraci and H. Wagner, Phys. Rev. B, 27 (1983) 5180.
[36] F. Houzay, G.M. Guichar, R. Pinchau, P. Thiry, Y. Petroff and D. Dagneaux, Surf. Sci., 99 (1980) 28.
[37] M. Giersig, M. Aggour and H.J. Lewerenz, to be published.
[38] H.J. Lewerenz, Electrochim. Acta, 37 (1992) 847.
[39] D.E. Aspnes, Am. J. Phys., 50 (1982) 704.
[40] G. Zuther, Phys. Status. Solidi A, 59 (1980) K 109.
[41] D.A.G. Bruggeman, Ann. Phys., 5 (1935) 636.